Biological Heating in the Equatorial Pacific: Observed Variability and Potential for Real-Time Calculation

PETER G. STRUTTON

State University of New York at Stony Brook, Stony Brook, New York

FRANCISCO P. CHAVEZ

Monterey Bay Aquarium Research Institute, Moss Landing, California

(Manuscript received 12 June 2002, in final form 22 August 2003)

ABSTRACT

Changes in phytoplankton concentration, mixed layer depth, and incident radiation strongly modify the upper-ocean heat budget. An extreme example occurred during the 1997/98 El Niño–La Niña. In the central equatorial Pacific, biological heating of the mixed layer increased from ~0.1°C month^{-1} in December 1997 (El Niño) to ~1.0°C month^{-1} in July 1998 (La Niña). This change was due to 1) shoaling of the mixed layer from ~100 to ~20 m (~56% of the 0.9°C month^{-1} increase); 2) a twentyfold increase in surface chlorophyll concentrations (~29% of the increase), coincident with a shoaling of the subsurface chlorophyll maximum from ~100 to ~50 m; and 3) an increase in incident shortwave radiation from ~175 to 275 W m^{-2} (~15% of the increase). The observed range of heating rates (0.1°–1.0°C month^{-1}) corresponds closely to the mean condition of the western (oligotrophic) and eastern (mesotrophic) equatorial Pacific, respectively. Increased phytoplankton concentrations act to retain heat near the surface and should result in shallower mixed layer depths. The influence of decadal changes in chlorophyll concentrations on heat storage was also quantified. The observed chlorophyll variability leads to interannual changes in penetrative heat flux ($E_{d,\mathrm{SW,PEN}}$, the irradiance flux out of the bottom of the mixed layer) of the order of 5 W m^{-2}, or from 65% to 170% of the mean. This variability is significant when compared with recent work that describes couplings between tropical and global ocean temperature dynamics. The analyses presented here show that satellite and buoy data can be used to accurately and simply estimate the biological contribution to heating for basin-scale studies, and possibly for future improvement of ocean circulation models.

1. Introduction

Heating of the oceanic mixed layer is influenced by 1) mixed layer depth, 2) the magnitude of incoming solar radiation, and 3) the biogenic content of the mixed layer (i.e., phytoplankton; Smith and Baker 1978; Sathyendranath et al. 1991). Changes in phytoplankton biomass do not affect the *total amount* of heat absorbed by the ocean—incoming solar radiation will be attenuated by the ocean whether or not phytoplankton are present. Rather, changes in mixed layer chlorophyll concentrations, through changes in the total chlorophyll inventory or its vertical distribution, impact the *partitioning* of heat between the mixed layer and deeper ocean. The need for better quantification of the biological contribution to mixed layer heating is particularly great in the equatorial Pacific because of the magnitude of interannual changes in phytoplankton biomass.

In the equatorial Pacific, mixed layer heating and SST are an intrinsic component of ocean–atmosphere interactions and El Niño–La Niña cycles—a phenomenon that has global climatic, ecological, and economic significance (Lehodey et al. 1997; Broad 1999; Chavez et al. 1999; McPhaden 1999; Behrenfeld et al. 2001). There is also mounting evidence that the physical variability of the equatorial Pacific is tightly coupled to global climate dynamics, at decadal to glacial time scales (Cane 1998; Zhang et al. 1998; Cole et al. 2000; Linsley et al. 2000a,b; Hoerling et al. 2001). Specifically, Cane (1998) noted that teleconnection mechanisms between the tropical Pacific and the global atmosphere are not unique to El Niño–La Niña events, and should occur similarly for SST variability occurring on longer time scales. Cole et al. (2000) concurred, suggesting that decadal variability in the tropical Pacific should force variability of similar time scales, wherever El Niño–La Niña teleconnections exist. Cane et al. (1997) went so far as to propose that coupling of this type between the tropical Pacific and the atmosphere was ''delaying and regulating global warming.''

In addition to its importance for climate, the equatorial Pacific is a globally significant component of bio-

Corresponding author address: Peter G. Strutton, Marine Sciences Research Center, State University of New York at Stony Brook, Stony Brook, NY 11794-5000.
E-mail: peter.strutton@sunysb.edu

geochemical cycles. The upwelling tongue that dominates the physical oceanography supplies high levels of nitrate but relatively little iron to the surface waters, thus giving rise to high nutrient–low chlorophyll (HNLC) conditions (Coale et al. 1996). The dynamics of the upwelling tongue, and its nutrient field, are perturbed by El Niño–La Niña cycles and significant fluctuations in primary productivity may result [decrease during El Niño, increase during La Niña; Barber et al. (1996); Chavez et al. (1996); Strutton and Chavez (2000)]. Given the importance of phytoplankton in the mixed layer heat budget, these changes in both the total phytoplankton biomass and its vertical distribution can significantly impact the way in which incident solar radiation is absorbed throughout the water column.

Previous work regarding the biological heating component of the equatorial Pacific heat budget has emphasized SST fluctuations in the western equatorial warm pool, because of the region's significance in modulating El Niño events (McPhaden et al. 1998). Siegel et al. (1995) demonstrated that the heat flux out of the bottom of the mixed layer ($E_{d,\mathrm{SW,PEN}}$) may be as much as 50% of the net flux at the surface, because the shallow mixed layer (~30 m) and low chlorophyll concentrations (~0.1 mg m^{-3}), which are common in the western equatorial warm pool, lead to low biological heating rates. The basin-scale analysis of Lewis et al. (1990) showed that for much of the central and eastern equatorial Pacific, $E_{d,\mathrm{SW,PEN}}$ was approximately equal to the net surface heat flux. This observation was offered as an explanation for the discrepancies between observed and modeled SSTs. Ohlmann et al. (1998, 2000) extended the work of Siegel et al. (1995) and examined the relative effects of chlorophyll concentration, zenith angle, and cloud cover on albedo, solar attenuation, and radiant heating in the upper 10–20 m of the ocean. Their results indicated that a tenfold change in chlorophyll throughout the upper 10 m of the ocean would result in the attenuation of an additional 10 W m^{-2} of incident irradiance, which equates to an additional heating of approximately 0.66°C $month^{-1}$. A tenfold change in chlorophyll is rare but feasible for the equatorial Pacific, given surface chlorophyll increased more than twenty-fold between January and July 1998 (Chavez et al. 1999; Strutton and Chavez 2000). Despite these efforts aimed at improving our understanding of biological heating, the chlorophyll contribution to heat budgets remains one of the most pressing issues to resolve in order to accurately model equatorial Pacific heat fluxes (Godfrey et al. 1998).

This work takes advantage of increasingly available satellite and mooring datasets, and a large database of conventional ship-based information to more accurately quantify the contribution of phytoplankton to heating within and below the mixed layer of the equatorial Pacific. We present calculations based on 1) conductivity–temperature–depth (CTD) profiles made between 8°N and 8°S, 180° and 95°W, and 2) the Sea-viewing Wide Field of View Sensor (SeaWiFS) satellite and Tropical Atmosphere–Ocean (TAO) mooring measurements of the entire region. Using these data, the aims of the paper are as follows:

1) To assess the accuracy of biological heating measurements made using satellite/mooring data.
2) To develop a simple operational framework for rapid calculation of pseudo–real-time biological heating rates.
3) To quantify the spatial and temporal variability of biological heating in the equatorial Pacific, with particular attention to the 1997/98 El Niño.
4) To quantify the relative contribution of chlorophyll concentration, mixed layer depth, and incident solar radiation to the observed variability.
5) To explore the potential role of decadal chlorophyll variability in deeper ocean heat storage.

2. Data and methods

a. Calculations from CTD profiles

In order to accurately describe the basin-scale dynamics of the equatorial Pacific heat budget, it was first necessary to develop a remote sensing approach to calculating radiant heating of the mixed layer. To achieve this, in situ cruise measurements of mixed layer heating were compared with calculations for the same locations obtained using only mooring and simulated satellite data.

The National Oceanic and Atmospheric Administration (NOAA) ship *Ka'imimoana* is dedicated to servicing the moorings of the TAO array. In the course of this work the ship performs CTDs to 1000 m, at least every degree of latitude between 8°N and 8°S along 95°, 110°, 125°, 140°, 155°, 170°W, 180°, and 165°E. Each station is visited twice annually, amounting to between 250 and 300 stations per year. Figure 1 shows the locations from which the CTD data used in this comparison were obtained. Since December 1997, chlorophyll and nutrient samples have been obtained at all of these stations, from eight depths between the surface and 200 m. Here, these chlorophyll data were interpolated at 1-m intervals in the vertical and used to quantify the contribution of biogenic material (mostly photosynthetic pigments) to the surface layer heat flux.

In the absence of reliable irradiance data for each CTD location, the SeaWiFS photosynthetically active/available radiation (PAR) product (400–700 nm, denoted $E_{d,\mathrm{PAR,0m+}}$) was used to estimate total shortwave solar radiation ($E_{d,\mathrm{SW,0m+}}$, ~285–2800 nm) at each CTD location. SeaWiFS $E_{d,\mathrm{PAR,0m+}}$ is available as 8-day averages, calculated following the method of Frouin and Chertock (1992). The satellite data were compared with $E_{d,\mathrm{SW,0m+}}$ data collected at 21 TAO array locations between September 1997 and February 2002 (more information available online at http://www.pmel.noaa.

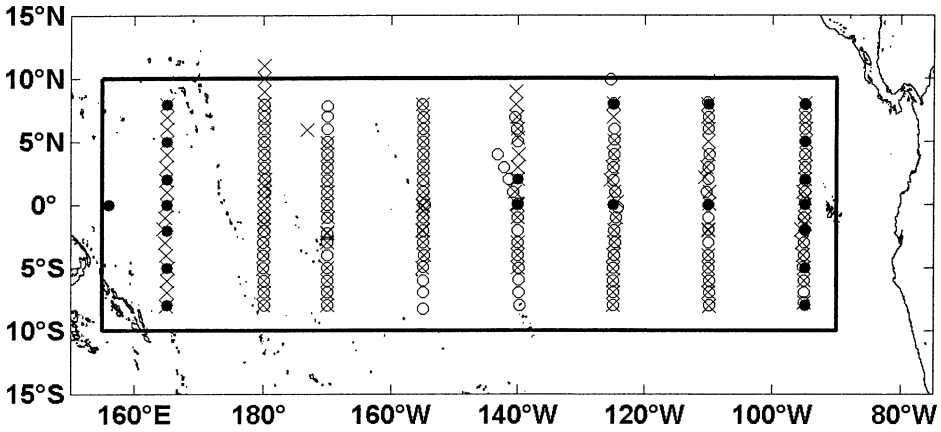

FIG. 1. Summary of the CTD station locations used to derive the relationship between mixed layer heating based on in situ data vs mooring/satellite data. The El Niño stations (○) span the period from 4 Oct 1997 to 6 Mar 1998, encompassing the maximum extent of the 1997/98 El Niño, while the La Niña stations (×) span 6 Jun–10 Nov 1998, covering the return to cool conditions which occurred in May 1998. Filled circles (●) indicate the location of TAO moorings from which shortwave radiation ($E_{d,\mathrm{SW},0\mathrm{m}+}$) data were obtained for determining the relationship between $E_{d,\mathrm{SW},0\mathrm{m}+}$ and SeaWiFS $E_{d,\mathrm{PAR},0\mathrm{m}+}$ (see Fig. 2). The rectangle spanning 10°N–10°S, 155°E–80°W indicates the region of the equatorial Pacific depicted in Fig. 4.

gov/tao/proj-over/sensors.shtml). These locations spanned the equatorial Pacific (Fig. 1), and the time period of data collection included both El Niño and La Niña conditions. Hence the derived relationship between $E_{d,\mathrm{PAR},0\mathrm{m}+}$ and $E_{d,\mathrm{SW},0\mathrm{m}+}$ (Fig. 2) includes spatial, seasonal, and interannual variability. The satellite data used for the comparison were the mean of all SeaWiFS 9-km pixels in a 1° × 1° box surrounding the mooring location of interest. The scatter about the linear trend is likely due to the effect of both clouds and solar zenith angle on the spectral shape of surface irradiance. Besides affecting the total amount of both $E_{d,\mathrm{PAR},0\mathrm{m}+}$ and $E_{d,\mathrm{SW},0\mathrm{m}+}$, clouds influence the spectral shape by skewing toward wavelengths less than 600 nm (Siegel et al. 1999). This skewing impacts $E_{d,\mathrm{SW},0\mathrm{m}+}$ more than $E_{d,\mathrm{PAR},0\mathrm{m}+}$, because a greater proportion of the $E_{d,\mathrm{SW},0\mathrm{m}+}$ spectrum exceeds 600 nm. This is likely the cause for the slight bias toward higher $E_{d,\mathrm{SW},0\mathrm{m}+}$ as $E_{d,\mathrm{PAR},0\mathrm{m}+}$ approaches 150 W m^{-2} in Fig. 2. Under clear-sky conditions, solar zenith angle contributes significantly to variability in both $E_{d,\mathrm{PAR},0\mathrm{m}+}$ and $E_{d,\mathrm{SW},0\mathrm{m}+}$. At high irradiance values, the effects of both cloud cover and solar zenith angle are minimized, which explains the reduced scatter in that portion of Fig. 2.

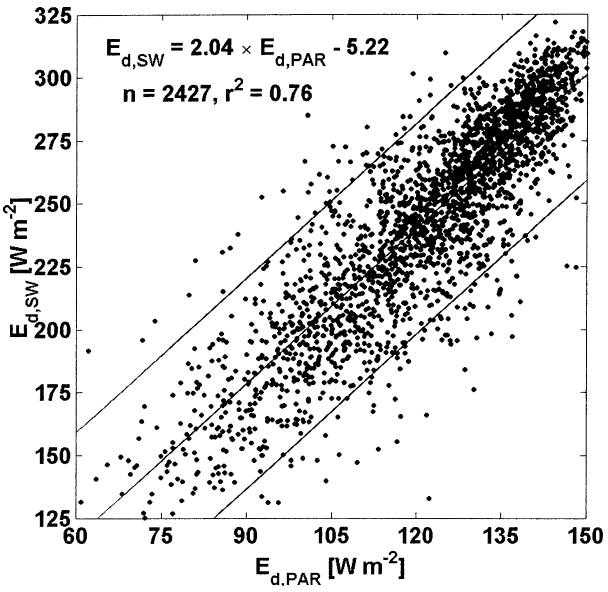

FIG. 2. Comparison of TAO shortwave radiation ($E_{d,\mathrm{SW},0\mathrm{m}+}$) and SeaWiFS $E_{d,\mathrm{PAR},0\mathrm{m}+}$ data compiled from 21 sites spanning 8°N–8°S, 156°E–95°W, for the period Sep 1997–Feb 2002. For each site, the SeaWiFS data are from a 1° × 1° box with the mooring location at the center. The linear relationship is plotted as well as the 95% confidence intervals.

For wavelengths greater than 700 nm, the diffuse attenuation due to pure water alone exceeds 0.5 m^{-1}, hence these wavelengths are almost completely attenuated within 10 m of the surface. Since all mixed layer depths of interest here are at least 10 m, wavelengths greater than 700 nm were not quantitatively propagated through the water column. In the physical oceanographic literature (e.g., Hayes et al. 1991; Wang and McPhaden 1999, 2000, 2001a,b) this is accounted for by multiplying $E_{d,\mathrm{SW},0\mathrm{m}+}$ by 0.45, before propagating through the water column using a constant diffuse attenuation coefficient, K, of 0.04 m^{-1}. That is

$$E_{d,\mathrm{SW},Z} = 0.45 \times E_{d,\mathrm{SW},0\mathrm{m}+} \times e^{-KZ}, \qquad (1)$$

where $E_{d,\mathrm{SW},Z}$ is the irradiance at depth Z. Using a bulk $E_{d,\mathrm{SW},0\mathrm{m}+}$ measurement at the surface (usually 220–229 W m^{-2} for the equatorial Pacific; Wang 1993) and then propagating that irradiance down through the mixed layer with a constant attenuation term in this fashion is not accurate, for two reasons. First, the energy at any individual wavelength changes inversely with wavelength

and second, the spectral distribution of solar radiation varies with depth. Hence, a spectral approach is necessary.

The biological heating calculation is described by

$$\left[\frac{dT}{dt}\right]_{\text{rad}} = \frac{E_{d,\text{SW},0\text{m}-} - E_{d,\text{SW,PEN}}}{\rho_0 C_p Z_{\text{MLD}}}, \quad (2)$$

where the left-hand side is the time rate of change of mixed layer temperature due to attenuation of downwelling irradiance (°C s^{-1}, but converted to °C month^{-1} below), $E_{d,\text{SW},0\text{m}-}$ and $E_{d,\text{SW,PEN}}$ are the total solar downwelling irradiance flux (W m^{-2}) immediately below the air–water interface and at the base of the mixed layer, respectively ($E_{d,\text{SW,PEN}}$ and $E_{d,\text{SW},Z_{\text{MLD}}}$ are equivalent).

The subscript SW is used to indicate that the entire shortwave spectrum is considered, but as described above, the contribution of wavelengths greater than 700 nm is negligible beyond 10-m depth. The density of seawater is represented by ρ_0(1022.4 kg m^{-3}), C_p is the heat capacity of seawater (4100 J kg^{-1} °C^{-1}) and Z_{MLD} is the depth of the mixed layer (m). Mixed layer depth was calculated as the depth at which temperature was 0.5°C less than SST (Anderson et al. 1996; Wang and McPhaden 1999, 2000, 2001a,b). In section 4c the errors in heating rate that could be caused by errors in the estimation of Z_{MLD} are discussed.

Equation (2) was implemented as follows:

1) The $E_{d,\text{PAR},0\text{m}+}$ for the time and location of each CTD cast was determined by linear interpolation of 8-day SeaWiFS $E_{d,\text{PAR},0\text{m}+}$ data. As for the comparison of SeaWiFS $E_{d,\text{PAR},0\text{m}+}$ and mooring $E_{d,\text{SW},0\text{m}+}$ (Fig. 2), the $E_{d,\text{PAR},0\text{m}+}$ data used to drive the heating calculations is the mean of a 1° × 1° box surrounding the location of interest.
2) The $E_{d,\text{PAR},0\text{m}+}$ was converted to $E_{d,\text{SW},0\text{m}+}$ using the relationship described in Fig. 2, and then to $E_{d,\text{SW},0\text{m}-}$ (shortwave radiation immediately below the water surface) using $E_{d,\text{SW},0\text{m}-} = (1 - \alpha)E_{d,\text{SW},0\text{m}+}$, where α is the albedo (α = 0.06; Payne 1972).
3) For the PAR portion of the spectrum, irradiance at wavelengths 400, 410, 420, . . . , 700 nm was determined as a function of the bulk $E_{d,\text{PAR},0\text{m}+}$ measurement. To achieve this spectral partitioning, optical data from 67 stations spanning ~8°N–8°S, ~90°W–180°, for the time period June 2000–October 2001 were analyzed. These profiles were obtained using a Satlantic Inc. SeaWiFS Profiling Multispectral Radiometer (SPMR), which measures 13 wavelengths (412–780 nm) of downwelling irradiance ($E_{d,\lambda}$) and upwelling radiance ($L_{u,\lambda}$) from both a floating surface sensor and an underwater profiling unit. Using only the above-water reference sensor irradiance data, the energy in each of the instrument's 13 wavelengths was quantified as a function of $E_{d,\text{PAR},0\text{m}+}$. This resulted in a spectrum of conversion factors that were then interpolated at 420, 430, 440, . . . , 700 nm and used to determine irradiance at these wavelengths for any given $E_{d,\text{PAR},0\text{m}+}$ measurement (Table 1). For 400 and 410 nm the values at 412 and 443 nm were linearly extrapolated.
4) The interpolated chlorophyll profile was then used to calculate the diffuse attenuation coefficient [$K(\lambda)$, λ = 400, 410, 420, . . . , 700 nm] at 1-m depth intervals to the bottom of the mixed layer using

$$K(\lambda) = K_w(\lambda) + K_{\text{BIO}}(\lambda) \quad \text{and} \quad (3)$$

$$K_{\text{BIO}}(\lambda) = (\chi)[\text{Chl}]^{e(\lambda)}, \quad (4)$$

where $K_w(\lambda)$ is the attenuation due to pure water and $K_{\text{BIO}}(\lambda)$ is the attenuation due to all biogenic components, including not only phytoplankton cells, but also bacteria, viruses, detritus and colored dissolved organic matter [see Eq. (3) in Morel and Maritorena 2001]. The wavelength-dependent values of K_w, χ and e, determined empirically from field data were used [see Eq. (5) and Table 2 in Morel and Maritorena 2001].
5) The $K(\lambda)$ profiles were then used to propagate each

TABLE 1. Factors for converting a bulk PAR measurement into irradiance at individual wavelengths. These data are based on means calculated from 67 optical profiles as described in the text. For the wavelengths measured, the std dev of the multiplier ranged from 1% to 3% of the mean. These factors vary slightly from those determined for extraterrestrial solar irradiance, due to the influence of clouds and water vapor in the atmosphere. When the corresponding factors for extraterrestrial irradiance were regressed against those above, the slope was 1.05 and the correlation was 0.83.

Wavelength (nm)	Multiplier
400	2.858e-03
410	3.000e-03
420	3.141e-03
430	3.283e-03
440	3.425e-03
450	3.514e-03
460	3.583e-03
470	3.652e-03
480	3.721e-03
490	3.790e-03
500	3.765e-03
510	3.729e-03
520	3.643e-03
530	3.599e-03
540	3.555e-03
550	3.511e-03
560	3.455e-03
570	3.405e-03
580	3.372e-03
590	3.339e-03
600	3.307e-03
610	3.274e-03
620	3.242e-03
630	3.215e-03
640	3.187e-03
650	3.160e-03
660	3.132e-03
670	2.984e-03
680	2.939e-03
690	2.813e-03
700	2.636e-03

wavelength (400, 410, 420, . . . , 700) to the bottom of the mixed layer. Total irradiance at the base of the mixed layer ($E_{d,\mathrm{SW},Z_{\mathrm{MLD}}}$ or $E_{d,\mathrm{SW,PEN}}$), was calculated by trapezoidal integration over the wavelength range.

It is important to note that the data presented here, in contrast to some previous studies, represent only the *biological component* of radiant heating due to both water and chlorophyll. That is, the calculations were performed twice: first with $K(\lambda) = K_W(\lambda) + K_{\mathrm{BIO}}(\lambda)$ to give *total radiant heating*, subsequently referred to as just *radiant heating*; and then with $K(\lambda) = K_W(\lambda)$ to give *radiant heating due only to attenuation by water*. (The difference of these two heating rates is presented in Figs. 4–6, and referred to as *biological radiant heating*, or simply *biological heating*.) In contrast to Wang and McPhaden (1999, 2000, 2001a,b), the calculations made here have not accounted for outgoing longwave radiation, latent and sensible heat fluxes, or advection.

b. Calculations using satellite and mooring data

The calculations of biological heating from simulated satellite data were performed as for the CTD profile data, with the following differences:

- Surface chlorophyll (as could be obtained from SeaWiFS) was converted to mean mixed layer chlorophyll using a relationship derived from 499 CTD stations occupied between October 1997 and August 1999, encompassing both El Niño and La Niña conditions and spanning the basin (Fig. 1):

$$\mathrm{Chl}_{\mathrm{MLD}} = \mathrm{Chl}_{\mathrm{SFC}} \times 0.9062 + 0.0354, \qquad r^2 = 0.86. \tag{5}$$

- Surface CTD chlorophyll data were used instead of actual SeaWiFS chlorophyll data so as to avoid complicating the comparison with issues of SeaWiFS retrieval accuracy. See section 4c for a discussion of potential errors related to the mixed layer chlorophyll estimation.
- Because a single bulk mixed layer chlorophyll was used, $E_{d,\mathrm{SW,0m-}}$ was propagated to the bottom of the mixed layer according to $E_{d,\mathrm{SW},Z_{\mathrm{MLD}}} = E_{d,\mathrm{SW,0m-}} \times \exp(-K Z_{\mathrm{MLD}})$. Here K was calculated spectrally (Morel and Maritorena 2001; see above), but did not vary as a function of depth.
- Mixed layer depth was calculated using the same temperature criterion (SST − 0.5°C), but using two different datasets: 1) the CTD temperature profile subsampled at the standard mooring temperature sensor depths to simulate a mooring profile, and 2) a temperature profile linearly interpolated from the nearest TAO mooring locations.

For both types of calculations, the minimum mixed layer depth was fixed at 10 m, for two reasons. First, TAO moorings are equipped with temperature sensors at 1.5 and 20 or 25 m, and so a temperature gradient (mixed layer boundary) at, say 10 or 20 m, when linearly interpolated between the two temperature sensors will almost certainly result in an erroneously shallow mixed layer depth. Second, extremely shallow mixed layers can result from calculations using either mooring or CTD data, if significant stratification occurs due to daily heating (Cronin and Kessler 2002). Time series data from 0°, 110°W clearly document this phenomenon, but also show that the mean daily mixed layer depth is seldom less than 10 m.

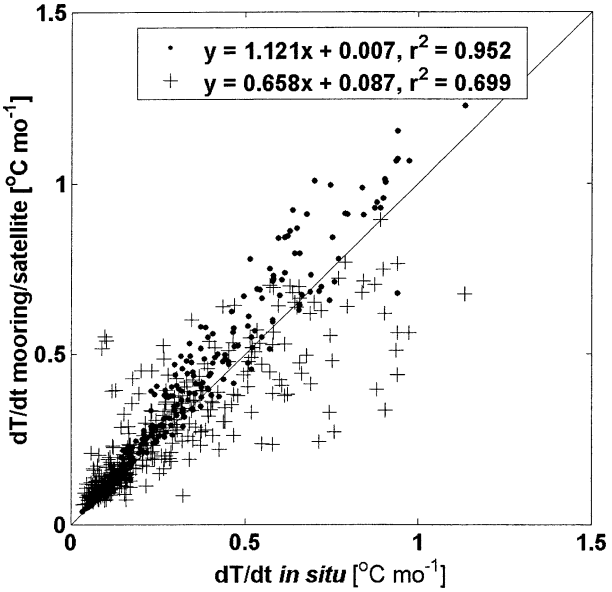

FIG. 3. Biological heating calculated using real-time data vs biological heating calculated using in situ data. For the real-time estimates, mixed layer depth was calculated using the temperature difference criterion described in the methods, applied to two different datasets: 1) the CTD temperature profile interpolated at the standard TAO temperature sensor depths, to simulate a mooring temperature profile (●), and 2) TAO temperature profiles averaged over a 5-day window and spatially interpolated to the location of the CTD (+). The difference in the strength of the correlation illustrates the impact of variability in mixed layer depth on the biological heating calculation.

Figure 3 shows the comparison between the CTD-derived and satellite/mooring biological heating estimates. The correlation between the two is much tighter, and the deviation from the one-to-one line is much less, for the mixed layer depth calculated from the subsampled CTD temperature profile as opposed to the interpolated TAO mooring profiles. This underscores the importance of mixed layer depth in modulating heating rates; that is, irradiance decreases exponentially with depth, so the numerator of Eq. (2) increases exponentially with depth. For the heating estimates made using TAO data to estimate mixed layer depth, the slope of the linear relationship with in situ data is 0.658, which indicates that this method underestimates biological heating at the higher end of the range. Comparison of

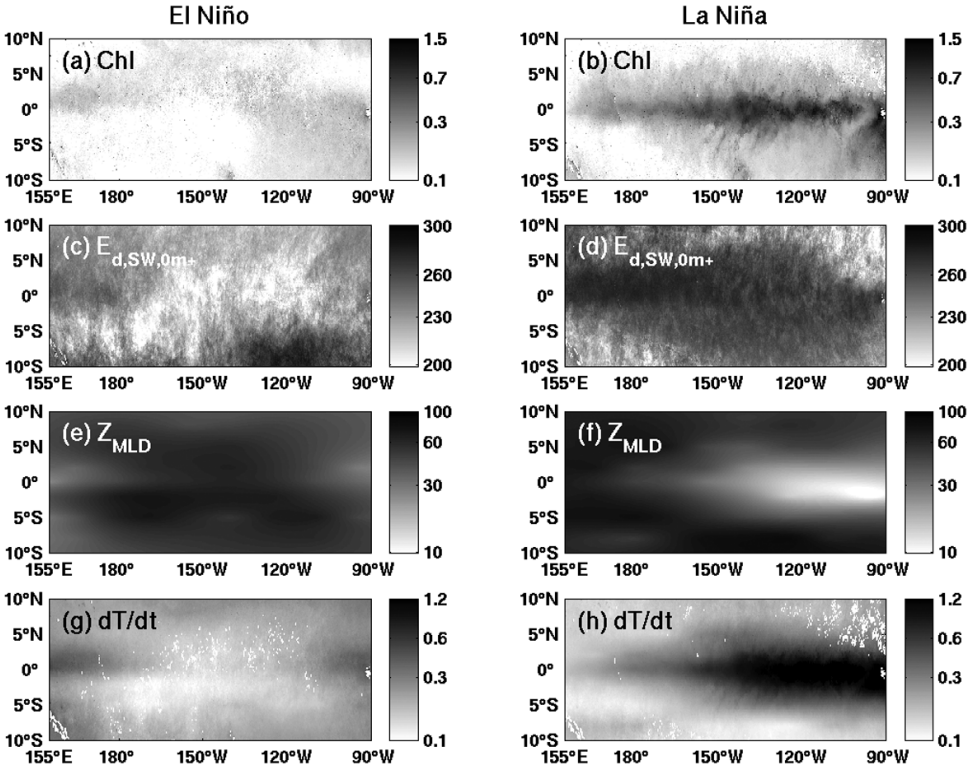

FIG. 4. (a), (c), (e), (g) Comparison of El Niño (Dec 1997–Feb 1998) and (b), (d), (f), (h) La Niña (Jul–Sep 1998) conditions. The parameters are (a), (b) mean SeaWiFS chlorophyll (Chl, mg m^{-3}); (c), (d) shortwave radiation ($E_{d,SW,0m+}$, W m^{-2}), calculated from SeaWiFS PAR using the relationship depicted in Fig. 2, (e), (f) mixed layer depth (Z_{MLD}, m), calculated from TAO mooring thermistor profile data using the temperature difference criterion described in the text (i.e., SST − 0.5°C); and (g), (h) biological heating (dT/dt, °C $month^{-1}$) calculated as described in the text. The dramatic increase in chlorophyll concentration as a result of the El Niño to La Niña transition has been well documented elsewhere (Chavez et al. 1999; Strutton and Chavez 2000; Ryan et al. 2002). The reduced solar radiation in the central Pacific during El Niño is due to the increased cloud cover associated with the eastward migration of the western warm pool. Comparison with Fig. 6 illustrates the relative contribution of mixed layer depth and chlorophyll concentration to the high heating rates observed in the eastern equatorial Pacific in mid-1998.

mixed layer depths calculated via the three different methods (CTD profile, subsampled CTD profile, and interpolated TAO data) confirmed that this underestimation of biological heating was due to an overestimation of mixed layer depth for mixed layers between 10 and 50 m. This is likely due to the depth distribution of the temperature sensors on the TAO moorings—the default is surface, 20/25 and 50 m. More temperature sensors in the upper 50 m would enhance the accuracy of mixed layer depth estimates and bring the slope in Fig. 3 closer to one.

For the purposes of describing the spatial and temporal variability of biological heating in the equatorial Pacific from 1997 to 2000, Fig. 3 shows that the satellite and mooring data can be used to obtain accurate estimates of biological heating, and for the remainder of this paper, these will be the data used.

3. Results

Chlorophyll concentrations in the equatorial Pacific increased more than twentyfold from some of the lowest (~0.05 mg m^{-3}, November 1997) to the highest (~1.0 mg m^{-3}, July 1998) levels ever observed for the region, as a result of the 1997/98 El Niño–La Niña transition (Chavez et al. 1999; Strutton and Chavez 2000; Ryan et al. 2002). Figures 4a,b provide a summary of the spatial and temporal chlorophyll variability observed by SeaWiFS between these two extremes. Based on these chlorophyll data, and using Eq. (5) in Morel and Maritorena (2001, with the parameters in their Table 2), the diffuse attenuation coefficient for the entire PAR spectrum (K_{PAR}) increased approximately threefold from ~0.04 to ~0.12 m^{-1} between El Niño and the peak of La Niña conditions [cf. Eq. (1) and the physical oceanographic literature which use $K_{PAR} = 0.04$ m^{-1}]. Shortwave radiation increased ~25% during the transition from El Niño to La Niña (Figs. 4c, d), as a result of the westward migration of the convective cell, and mixed layer depths shoaled (Figs. 4e, f), most notably in the central and eastern Pacific (McPhaden 1999). The changes in chlorophyll, shortwave radiation, and mixed layer depth combined to cause a huge increase in bio-

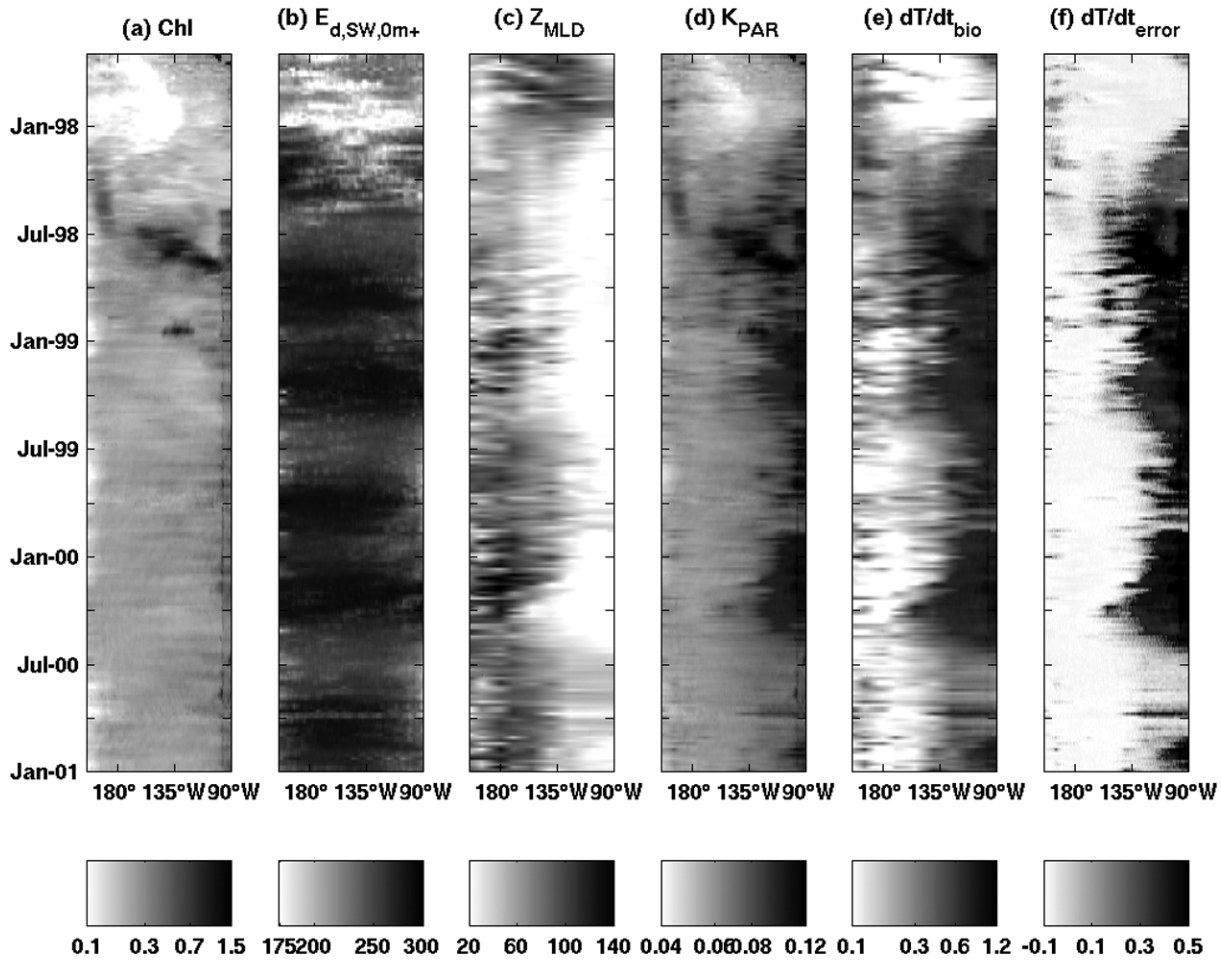

FIG. 5. Longitude–time sections along the equator, spanning the peak of the 1997/98 El Niño event and the extended La Niña conditions from the middle of 1998 onward. The parameters represented are (a) SeaWiFS chlorophyll (Chl, mg m^{-3}), averaged from 2°N to 2°S; (b) incident shortwave radiation ($E_{d,SW,0m+}$, W m^{-2}), also averaged from 2°N to 2°S and derived from SeaWiFS PAR data as described in methods; (c) mixed layer depth (Z_{MLD}, m) calculated from TAO moorings spanning 2°N to 2°S; (d) the diffuse attenuation coefficient of PAR (K_{PAR}, m^{-1}) based on chlorophyll and averaged over the mixed layer; (e) the biological heating rate (dT/dt_{bio}, °C $month^{-1}$) calculated using the Z_{MLD}, Chl, and $E_{d,SW,0m+}$ data presented; and (f) the difference (°C $month^{-1}$) between dT/dt_{bio} and the biological heating rate calculated assuming a constant K_{PAR} of 0.04 m^{-1}.

logical heating, most notably in the central and eastern Pacific (Figs. 4g,h).

Viewed in the context of longer time-scale variability spanning October 1997 to the end of 2000 (Fig. 5), the dramatic changes depicted in Fig. 4 are clearly visible, as well as some obvious seasonal signals. Shortwave radiation experiences local minima around January and July each year that are more significant in the west and east of the basin, compared to the central Pacific (Fig. 5b). The westward expansion of the shallow mixed layer region in the east of the basin around March each year coincides with the ''springtime reversal'' of the South Equatorial Current (SEC; Halpern 1987; McPhaden and Taft 1988) and a general warming of that region (Fig. 5c). In contrast to $E_{d,SW,0m+}$ and Z_{MLD}, the seasonal variability in chlorophyll concentration for this time period is minimal, with concentrations generally in excess of 0.2 mg m^{-3} from mid-1998 onward over almost the entire basin, as a result of persistent upwelling conditions (Fig. 5a). The spatial and temporal patterns in K_{PAR} (Fig. 5d) closely resemble that of chlorophyll, but also incorporate some variability due to Z_{MLD} because K_{PAR} was calculated spectrally, and the depth of penetration is a function of wavelength. Figure 5e shows the biological heating rates corresponding to the physical and biological variability shown in Figs. 5a–5d. For comparison, Fig. 5f shows the errors ($dT/dt_{bio} - dT/dt_{phys}$) that would result had biological heating been calculated using a constant K_{PAR} of 0.04 m^{-1}, as in the physical oceanographic literature. In the eastern Pacific this results in an underestimate of approximately 50%.

Shallow mixed layers are associated with high heating rates because of the presence of Z_{MLD} in the denominator of Eq. (2). This is clearly visible in the eastern equatorial Pacific (Figs. 4 and 5). However, shallow mixed layers also increase the sensitivity of the biological heating

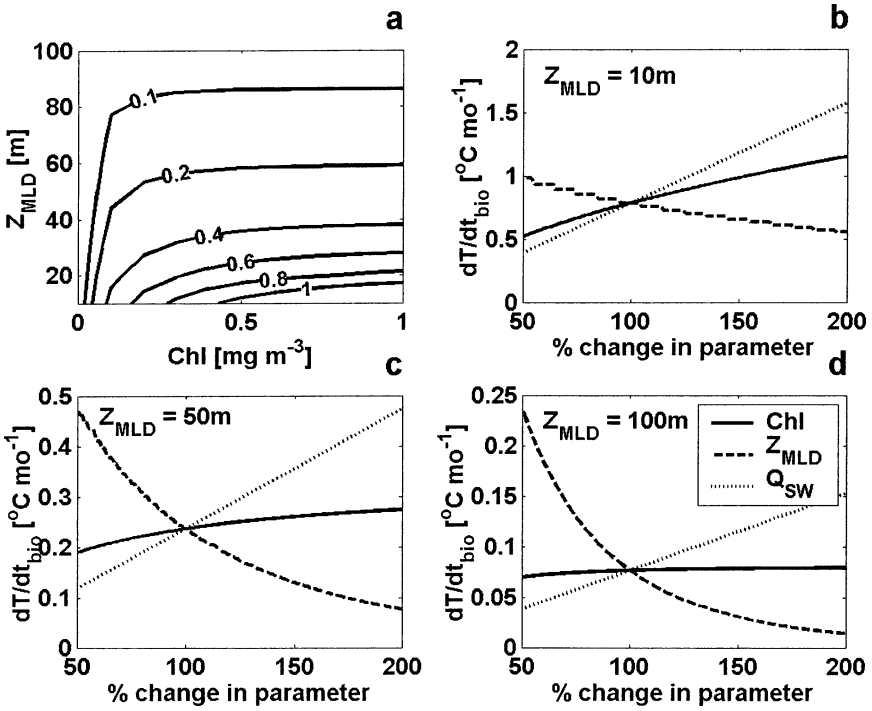

FIG. 6. (a) The dependence of biological heating (plotted as contours in °C month^{-1}) on chlorophyll concentration and mixed layer depth. Biological heating is most sensitve to variability in chlorophyll concentration at shallow mixed layer depths. El Niño conditions are best represented by the left and upper left of the diagram (low chlorophyll, intermediate to deep mixed layers), while eastern Pacific La Niña conditions most closely resemble the bottom right of the figure (high chlorophyll, shallow mixed layer). (b), (c), (d) The error in the biological heating calculation caused by a factor of 2 error in chlorophyll, Z_{MLD}, and $E_{d,SW,0m+}$.

equation to changes in chlorophyll. Figure 6a and Table 2 summarize the dependence of biological heating on mixed layer depth and chlorophyll concentration. For deep mixed layers (50–100 m), a change in mixed layer chlorophyll concentration from 0 to 1 mg m^{-3} results in almost no change to the resulting biological heating rate, because the attenuation due to water dominates any variability in the biological attenuation [see Eq. (3)]. Put another way, when the mixed layer is deep, attenuation by pure water absorbs the majority of the incoming solar radiation, so any additional variability in the attenuation due to chlorophyll has little impact on heating. However for shallow mixed layers of 20–40 m, variability in chlorophyll of the magnitude seen during the transition from El Niño to La Niña conditions has a significant impact. During the IronEx II experiment, Kudela and Chavez (1996) observed an increase in chlorophyll of approximately 0.2–2.0 mg m^{-3} for a mixed layer depth of ~40 m, and calculated an increase in biological heating of 0.27°C month^{-1}. This calculation roughly concurs with Fig. 6a, which indicates an increase of ~0.3°C month^{-1} for IronEx II conditions. Fig-

TABLE 2. Biological heating rate as a function of mixed layer chlorophyll concentration (mg m^{-3}) and mixed layer depth (m). The chlorophyll concentrations were chosen to represent seawater only (0 mg m^{-3}), extremely oligotrophic or strong El Niño conditions (0.05 mg m^{-3}), the mean condition for the equatorial Pacific (0.2 mg m^{-3}), and high chlorophyll or La Niña bloom conditions (0.6 mg m^{-3}). The mixed layer depths were chosen to represent the shallowest observed for the eastern Pacific (10 m), the basin-wide mean (50 m) and the western Pacific (100 m). Data presented are mixed layer radiant heating rates (due to water *and* chlorophyll) in °C month^{-1} (left-hand column under each Z_{MLD} heading) and the same rate expressed as a radiative heat flux (Q_{RAD}; W m^{-2}) absorbed in the mixed layer (right-hand column under each Z_{MLD} heading). The penetrative heat flux ($E_{d,SW,PEN}$) for each Chl/Z_{MLD} combination can be calculated by subtracting Q_{RAD} from the shortwave radiation flux ($E_{d,SW,0m-}$) just below the water surface (0.94 × 229 = 215.26 W m^{-2}).

	Chl (mg m^{-3})	Z_{MLD} = 10 m		Z_{MLD} = 50 m		Z_{MLD} = 100 m	
Nonspectral	K = 0.04 m^{-1}	9.17	146.16	2.53	201.36	1.34	213.36
"Pure" seawater	0	10.06	160.40	2.40	191.04	1.27	202.51
Oligotrophic/El Niño	0.05	10.40	165.84	2.54	202.27	1.33	211.90
Mesotrophic/mean	0.2	10.85	173.00	2.63	209.98	1.35	214.75
Bloom/La Niña	0.6	11.48	183.05	2.69	214.03	1.35	215.23

ures 6b,c,d illustrate the variability in biological heating as a function of variability in Z_{MLD}, chlorophyll, and $E_{d,SW,0m+}$. Chlorophyll and $E_{d,SW,0m+}$ were varied by a factor of 2 about mean values of 0.2 mg m^{-3} and 229 W m^{-2} (Wang 1993) for Z_{MLD} = 10, 50, and 100 m, respectively. At each of these Z_{MLD} values, Z_{MLD} was also varied by a factor of 2. For Z_{MLD} = 10 m, increasing Chl from 0.1 to 0.4 mg m^{-3} results in a more than doubling of biological heating from ~0.5° to ~1.2°C month^{-1}. For Z_{MLD} = 50 m, the increase is less than 0.1°C month^{-1}, while for Z_{MLD} = 100 m, it is negligible.

4. Discussion

a. Seasonal, interannual, and spatial variability in biological heating

Under conditions of moderate or strong upwelling, the eastern equatorial Pacific is characterized by high chlorophyll, cool SST, and a shallow thermocline, while lower chlorophyll, warmer SST, and a deeper thermocline are typical of the west. It is this zonal difference in chlorophyll and thermocline/mixed layer depth that is largely responsible for the east to west decrease in heating rates observed in Figs. 4 and 5. This results in the coolest SST waters experiencing the highest heating rates. Between December 1997 (El Niño) and June 1998 (La Niña), the central equatorial Pacific was transformed from a state resembling the mean condition of the oligotrophic western Pacific to that resembling the mesotrophic eastern equatorial Pacific. This transition caused an increase in the biological heating rate from approximately 0.1° to 1.0°C month^{-1}. Approximately 56% of this 0.9°C month^{-1} increase was accounted for by the change in mixed layer depth, while the increase in chlorophyll and shortwave radiation accounted for 29% and 15% of the increase, respectively.

Using a constant attenuation term of 0.04 m^{-1} (i.e., not accounting for changes in chlorophyll concentrations), Wang and McPhaden (1999) reported mean annual mixed layer heating rates (i.e., adjusted net surface heat flux) for the eastern Pacific (0°, 110°W) that were almost eightfold higher than in the west (0°, 165°E). Including the effect of increasing chlorophyll from west to east would have magnified this difference in their results. By analogy with the results presented here, assuming a constant attenuation term would have missed 29% of the variability in radiant heating observed during the 1997/98 El Niño to La Niña transition. Associated with this zonal gradient, Wang and McPhaden (1999) also showed that the magnitude of the seasonal variability in heating rates decreased more than threefold from east to west and that the net surface heat flux was generally the largest term in the surface layer heat budget. This underscores the importance of calculating mixed layer radiant heating accurately, since the surface fluxes are at least partly dependent on the ocean–atmosphere gradient.

At interannual time scales Wang and McPhaden (2000, 2001a) emphasized the importance of the vertical turbulent heat flux out of the bottom of the mixed layer (i.e., Q_W, not $E_{d,SW,PEM}$), particularly in the eastern Pacific at the termination of the 1997/98 El Niño, when the mixed layer was very shallow. Based on this observation it was suggested that zonal advection was not as important in governing El Niño termination as previously thought (Picaut et al. 1997). Using a constant attenuation coefficient of 0.04 m^{-1}, Wang and McPhaden (2001a) would have underestimated the heating of the mixed layer in 1998 by ~40 W m^{-2} (Table 2), and so overestimated Q_W by the same amount since it was calculated as a residual [see their Eq. (3)]. This overestimation may have influenced their conclusion regarding the relative importance of vertical versus horizontal fluxes.

b. Incorporation of variable biological heating into models

Recently, Nakamoto et al. (2001) incorporated variable biological heating (according to Morel and Antoine 1994) into an ocean general circulation model, and compared the resulting SST field with the same model using a constant mixed layer heating parameterization similar to Hayes et al. (1991). For the equatorial Pacific (Nakamoto et al. 2001) the incorporation of realistic biological heating shoaled the mixed layer by trapping heat closer to the surface. This observation serves as an interesting comparison with Ohlmann et al. (1998), who described a feedback mechanism whereby a shallower mixed layer favors more heat penetration below the mixed layer, thus destabilizing and deepening the mixed layer. Interestingly, Nakamoto et al. (2001) showed that enhanced biological heating ultimately leads to cooler SSTs in the eastern Pacific because of enhanced westward surface currents, which strengthen the equatorial undercurrent and favor upwelling.

Murtugudde et al. (2002) also compared circulation models using constant *versus* variable (biological) attenuation. In the eastern equatorial Pacific, the biological model resulted in increased loss of heat to the subsurface, but also increased SST. This increased subsurface heating due to biology led to decreased upwelling (cf. increased upwelling in Nakamoto et al. 2001) because of weaker stratification, deeper mixed layers, and reduced divergence. The contrasting results of these two studies may largely result from 1) differences in the physical circulation models and 2) differences in the control conditions against which the variable attenuation models were compared. Nakamoto et al. (2001) used an attenuation depth of 23 m (K_{PAR} = 0.043 m^{-1}) for their control runs while Murtugudde et al. (2002) used 17 m (K_{PAR} = 0.059 m^{-1}). Using a coupled ocean–atmosphere model, Timmermann and Jin (2003) showed that elevated chlorophyll concentrations during La Niña events imparted a negative feedback by increasing attenuation, heating, and SST. When compared with their control

situation ($K_{PAR} = 0.043\ m^{-1}$), sensitivity to chlorophyll increased SST during La Niña by up to 2°C, but did not change the duration of La Niña events.

At a global scale Rochford et al. (2001) showed that incorporating realistic biological heating, derived from available satellite data, improved the SST predictive skill of a general circulation model, most notably in the Tropics. In midlatitudes, such as the open-ocean gyres where chlorophyll concentrations are relatively low and invariant, adding a biological component to the model had little effect. In contrast to previous work that has used $K_{PAR} = 0.04\ m^{-1}$ as a good ''general purpose'' estimate of attenuation, Rochford et al. (2001) showed that $K_{PAR} = 0.06\ m^{-1}$ works very well over vast regions of the ocean. A value of $0.06\ m^{-1}$ is in the middle of the range of values depicted in Fig. 5, corresponding to mesotrophic conditions typically observed near ~120°W. Rather than using a fixed attenuation value, the accuracy of the biological heating component in physical circulation models could be significantly improved by incorporating the technique described in section 2b. This would require chlorophyll (or attenuation) data as input, that is, annual or perhaps monthly climatologies, or real-time estimates from a coupled biological model.

c. *Mooring/satellite-based estimates of biological heating—Sources of error*

Given the climatic and economic impact of strong El Niño events (Bakun 1996; Broad 1999), it is important to predict their timing and magnitude as accurately as possible, and to do this requires reliable models. Lewis et al. (1990) suggested that the biological component of the equatorial Pacific heat budget explained the discrepancy between modeled and observed SSTs, thus emphasizing the need to accurately and easily estimate biological heating at the basin scale. The almost real-time availability of SeaWiFS surface chlorophyll distributions and mooring temperature profiles should make such calculations possible.

Figure 3 quantifies the success of a first attempt at deriving biological heating using available real-time data. While the correlations with the more accurate ship-based estimates are encouraging, the major source of variability is differences in the Z_{MLD} estimates. Overestimating Z_{MLD} by 50% results in an underestimate of biological heating of between 25% for a shallow mixed layer (Fig. 6b) and 50% for a deeper mixed layer (Fig. 6d). The corresponding overestimates of biological heating for underestimating Z_{MLD} are as great as 300% for $Z_{MLD} = 100$ m (Fig. 6d). Miscalculating Z_{MLD} by 50% perhaps represents an extreme case—for a chlorophyll concentration of 0.5 mg m^{-3} and a mixed layer depth of 20 m, an error in Z_{MLD} of 1 m results in a biological heating error of 0.05°C $month^{-1}$, or approximately 4% (Fig. 7). For the same chlorophyll concentration and a mixed layer depth of 100 m, an error in Z_{MLD} of 1 m

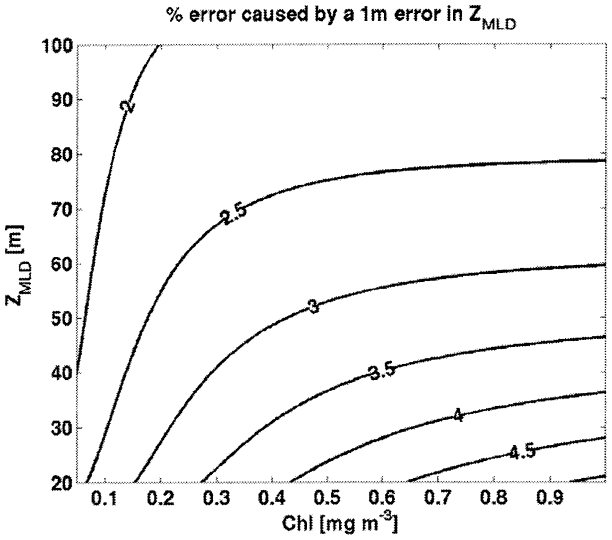

FIG. 7. The percentage error in biological heating (plotted as contours) caused by a 1-m error in the estimation of Z_{MLD}, plotted as a function of chlorophyll and Z_{MLD}. Biological heating is most sensitive to variability in Z_{MLD} at shallow mixed layer depths and high chlorophyll concentrations.

results in ~2% error in the biological heating rate. Given the potential importance of salinity in determining Z_{MLD} (particularly in the western Pacific), obtaining the best possible Z_{MLD} estimates remains problematic, but could be helped by incorporating either increased coverage of salinity data on the TAO array or empirical relationships between temperature gradients and mixed layer depths based on CTD-derived climatologies.

The sensitivity of the biological heating calculation to $E_{d,SW,0m+}$ is linear, and given the accuracy with which this parameter can be measured from space (Frouin and Chertock 1992), errors in $E_{d,SW,0m+}$ are unlikely to significantly impact biological heating estimates. The same is true of chlorophyll, but to a lesser extent, because Fig. 6b shows that for shallow mixed layers, errors in chlorophyll can significantly impact the resulting biological heating estimate. The data presented in Figs. 4 and 5 relied on a relationship that estimated mean mixed layer chlorophyll (Chl_{MLD}) from surface chlorophyll (Chl_{SFC}). The errors associated with this relationship are such that for $Chl_{SFC} = 0.05$ mg m^{-3} the standard error of Chl_{MLD} is 40%, which in the most extreme case (shallow mixed layer, $Z_{MLD} \sim 20$ m) leads to an error in heating rate of 0.05°C $month^{-1}$, or 20%. For $Chl_{SFC} = 0.5$ mg m^{-3} the corresponding maximum error in heating rate is 0.02°C $month^{-1}$, or 2%.

d. *Significance of long-term changes in chlorophyll concentration*

The 1997/98 El Niño event was by some measures the strongest ever observed (McPhaden 1999), and the parameters influencing biological heating underwent ex-

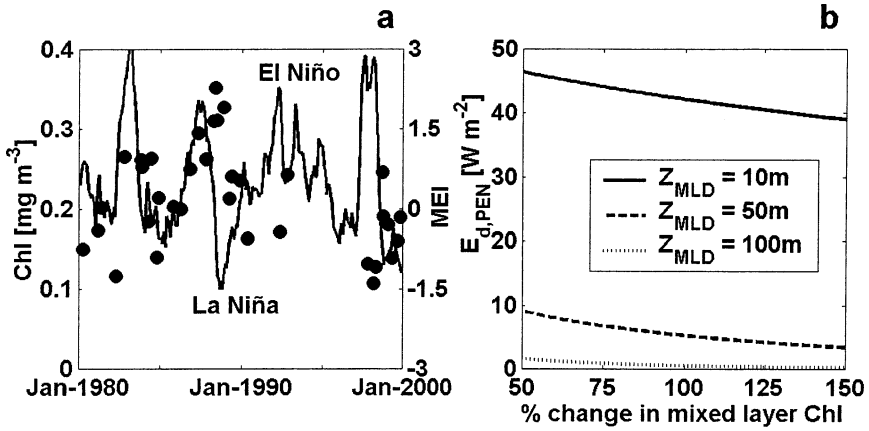

FIG. 8. (a) Mean chlorophyll concentration in a box bounded by 1°N–1°S, 110°–140°W since 1980. The mean chlorophyll concentration for all cruises in the MBARI database is 0.21 mg m^{-3} (Chavez et al. 1999)—note that the data presented here vary by approximately 50% of this value. On the right-hand axis, the multivariate ENSO index (MEI; Wolter and Timlin 1998) is plotted. Positive values indicate El Niño events, and negative values indicate La Niña. (b) Total heat flux penetrating the bottom of the mixed layer ($E_{d,\mathrm{SW,PEN}}$, or penetrative heat flux), as a function of a 50% change in the mean chlorophyll concentration of the mixed layer, for mixed layer depths of 10, 50, and 100 m.

treme perturbations. Thus it is important to quantify the changes in biological heating resulting from less dramatic physical forcing that the region may more typically experience. Measurements made since 1980 (a subset of which is plotted in Fig. 8a), show variability in equatorial Pacific chlorophyll of the order of 50% about a mean of 0.21 mg m^{-3} (see Fig. 7 in Chavez et al. 1999). Fluctuations of this magnitude should impact the heat budget of the equatorial Pacific, such that increases in mixed layer chlorophyll would increase biological heating in the mixed layer, and decrease $E_{d,\mathrm{SW,PEN}}$, the penetrative heat flux out of the bottom of the mixed layer. Using a climatological $E_{d,\mathrm{SW},0\mathrm{m}+}$ of 229 W m^{-2} (Wang 1993), the changes in $E_{d,\mathrm{SW,PEN}}$ associated with changes in mean mixed layer chlorophyll of $\pm 50\%$ about 0.21 mg m^{-3} were calculated using $E_{d,\mathrm{SW,PEN}} = E_{d,\mathrm{SW},0-}e^{-KZ}$, where K was obtained using Eqs. (3) and (4). For conditions resembling the eastern Pacific ($Z_{\mathrm{MLD}} \sim 10$ m), $E_{d,\mathrm{SW,PEN}}$ decreases from 46.5 to 39.0 W m^{-2} in response to an increase in mixed layer chlorophyll from 0.1 to 0.3 mg m^{-3}. For a basin-wide mean mixed layer of 50 m (da Silva et al. 1994), $E_{d,\mathrm{SW,PEN}}$ ranges from 9.1 to 3.4 W m^{-2} about a mean of 5.3 W m^{-2} in response to the same chlorophyll increase. As described above, chlorophyll variability has little impact on the partitioning of biological heating for deep mixed layers, and for $Z_{\mathrm{MLD}} = 100$ m, the corresponding decrease in $E_{d,\mathrm{SW,PEN}}$ is from 1.6 to 0.2 W m^{-2}.

The obvious question for the physical oceanographers is ''are these fluctuations significant?'' and more generally ''How might these changes influence interannual temperature variability in the tropical Pacific and perhaps elsewhere?'' White et al. (2001) showed that during the onset phase of El Niño events, the observed warming of the Tropics was caused primarily by a reduction in the poleward heat flux from the equatorial ocean of the order of 2–5 W m^{-2}. The biologically mediated variability in $E_{d,\mathrm{SW,PEN}}$ for a mean mixed layer of 50 m and realistic or even minimal changes in chlorophyll concentration is more than 5 W m^{-2}. Thus, it appears that biologically mediated variability in the mixed layer heat budget is significant and should be accounted for. Furthermore, the magnitude of the chlorophyll variability shown in Fig. 8 is probably small relative to the changes on glacial–interglacial cycles (Paytan et al. 1996; Wells et al. 1999), which suggests this effect could be even more significant than shown here at these longer time scales.

5. Conclusions

As a result of the extreme fluctuations in chlorophyll and mixed layer depth during the 1997/98 El Niño, mixed layer biological heating rates in the central equatorial Pacific increased from 0.1° in late 1997 to 1.0°C $month^{-1}$ in July 1998. Changes in surface downwelling irradiance ($E_{d,\mathrm{SW},0\mathrm{m}+}$) also contributed to this phenomenon, but were of lesser importance. Investigation of long-term fluctuations in chlorophyll concentrations illustrates that the chlorophyll variability more routinely observed in the equatorial Pacific can lead to significant changes in mixed layer biological heating, and, perhaps more importantly, the penetrative heat flux ($E_{d,\mathrm{SW,PEN}}$) through the mixed layer into the deeper ocean. These longer time-scale processes may significantly impact the interannual physical variability of the region, and should be accounted for in physical models. Currently available satellite chlorophyll data, and the algorithm relating surface chlorophyll to mixed layer chlorophyll, are sufficiently accurate for this purpose. The determination of

APPENDIX

List of Symbols

Symbol	Definition	Units
α	Albedo	Dimensionless
$\chi(\lambda)$	Multiplier for Chl in Eq (4)	Dimensionless
ρ_0	Density of seawater	1022.4 kg m^{-3}
Chl	Chlorophyll concentration	mg m^{-3}
Chl_{MLD}	Mean mixed layer chlorophyll concentration	mg m^{-3}
Chl_{SFC}	Surface chlorophyll concentration	mg m^{-3}
C_p	Specific heat of seawater	J kg^{-1} °C^{-1}
$e(\lambda)$	Exponent for Chl in Eq (4)	Dimensionless
$E_{d,PAR,0m-}$	PAR immediately below the surface	W m^{-2}
$E_{d,PAR,0m+}$	PAR immediately above the surface	W m^{-2}
$E_{d,SW,0m-}$	Shortwave radiation immediately below the surface	W m^{-2}
$E_{d,SW,0m+}$	Shortwave radiation immediately above the surface	W m^{-2}
$E_{d,SW,PEN}$	Irradiance penetrating below the mixed layer	W m^{-2}
K	Diffuse attenuation coefficient	m^{-1}
$K(\lambda)$	Diffuse attenuation coefficient	m^{-1}
$K_{BIO}(\lambda)$	Diffuse attenuation coefficient due to biogenic material	m^{-1}
K_{PAR}	Diffuse attenuation coefficient of PAR	m^{-1}
$K_w(\lambda)$	Diffuse attenuation coefficient due to pure water	m^{-1}
PAR	Photosynthetically available/active radiation	W m^{-2}
Q_{RAD}	Radiant heat flux (into the mixed layer)	W m^{-2}
Q_w	Vertical turbulent diffusive heat flux (out of the mixed layer)	W m^{-2}
T	Temperature	°C
t	Time	s
Z	Depth	m
Z_{MLD}	Mixed layer depth	m

mixed layer depths is more problematic, but could be improved by 1) greater resolution of TAO temperature measurements in the upper 50 m in the eastern Pacific, and 2) widespread deployment of salinity sensors in the western Pacific.

Acknowledgments. A large portion of the chlorophyll data used to calculate the CTD-based heating rates were collected by volunteers aboard the NOAA ship *Ka'imimoana*, in particular, Jason Kahn, Kimberly Baldwin, Kate Treese, and Peter Bernhardt. Cynthia Venn assisted with cruise logistics for the volunteers. Dennis Sweeney, Brian Powers, and the officers and crew of the *Ka'imimoana* gave their customary excellent support at sea. The SeaWiFS chlorophyll and PAR data were obtained from the Distributed Active Archive Center (http://daac.gsfc.nasa.gov/). Equatorial Pacific mooring data were obtained from the TAO project, Michael McPhaden, director (http://www.pmel.noaa.gov). Weimin Wang, Dave Siegel, Carter Ohlmann, Meghan Cronin, Robert Maffione, Zanna Chase, and three anonymous reviewers provided valuable comments on earlier drafts of the manuscript. Financial support for this work came from the NASA SIMBIOS program, NOAA's Office of Global Programs, and the David and Lucile Packard Foundation.

REFERENCES

Anderson, S. P., R. A. Weller, and R. B. Lukas, 1996: Surface buoyancy forcing and the mixed layer of the western Pacific warm pool: Observations and 1D model results. *J. Climate,* **9,** 3056–3085.

Bakun, A., 1996: Patterns in the ocean: Ocean processes and marine population dynamics. California Sea Grant College System Rep. T-037, La Jolla, California, 323 pp.

Barber, R. T., M. P. Sanderson, S. T. Lindley, F. Chai, J. Newton, C. C. Trees, D. G. Foley, and F. P. Chavez, 1996: Primary productivity and its regulation in the equatorial Pacific during and following the 1991–1992 El Niño. *Deep-Sea Res.,* **43B,** 933–969.

Behrenfeld, M. J., and Coauthors, 2001: Biospheric primary production during an ENSO transition. *Science,* **291,** 2594–2597.

Broad, K., 1999: Climate, culture and values: El Niño 1997–98 and Peruvian fisheries. Ph.D. dissertation, Department of Anthropology, Columbia University, New York, NY, 311 pp.

Cane, M. A., 1998: Climate change: A role for the tropical Pacific. *Science,* **282,** 59–61.

——, A. C. Clement, A. Kaplan, Y. Kushnir, D. Pozdnyakov, R. Seager, S. E. Zebiak, and R. Murtugudde, 1997: Twentieth-century sea surface temperature trends. *Science,* **275,** 957–960.

Chavez, F. P., K. R. Buck, S. K. Service, J. Newton, and R. T. Barber, 1996: Phytoplankton variability in the eastern and central tropical Pacific. *Deep-Sea Res.,* **43B,** 835–870.

——, P. G. Strutton, G. E. Friederich, R. A. Feely, G. C. Feldman, D. G. Foley, and M. J. McPhaden, 1999: Biological and chemical response of the equatorial Pacific Ocean to the 1997–98 El Niño. *Science,* **286,** 2126–2131.

Coale, K. H., and Coauthors, 1996: A massive phytoplankton bloom induced by an ecosystem-scale iron fertilization experiment in the equatorial Pacific Ocean. *Nature,* **383,** 495–501.

Cole, J. E., R. B. Dunbar, T. R. McClanahan, and N. A. Muthiga, 2000: Tropical Pacific forcing of decadal SST variability in the western Indian Ocean over the past two centuries. *Science,* **287,** 617–619.

Cronin, M. F., and W. S. Kessler, 2002: Seasonal and interannual modulation of mixed layer variability at 0°, 110°W. *Deep-Sea Res.,* **49A,** 1–17.

da Silva, A. M., C. C. Young, and S. Levitus, 1994: *Algorithms and*

Procedures. Vol. 1, *Atlas of Surface Marine Data 1994*. NOAA Atlas NESDIS 6, U.S. Department of Commerce, 83 pp.

Frouin, R., and B. Chertock, 1992: A technique for global monitoring of net solar irradiance at the ocean surface. Part I: Model. *J. Appl. Meteor.*, **31,** 1056–1066.

Godfrey, J. S., R. A. Houze Jr., R. H. Johnson, R. Lukas, J. L. Redelsperger, A. Sumi, and R. Weller, 1998: Coupled Ocean–Atmosphere Response Experiment (COARE): An interim report. *J. Geophys. Res.*, **103,** 14 395–14 450.

Halpern, D., 1987: Observations of annual and El Niño thermal and flow variations at 0°, 110°W and 0°, 95°W during 1980–1985. *J. Geophys. Res.*, **92,** 8197–8212.

Hayes, S. P., P. Chang, and M. J. McPhaden, 1991: Variability of the sea surface temperature in the eastern equatorial Pacific during 1986–88. *J. Geophys. Res.*, **96,** 10 553–10 566.

Hoerling, M. P., J. W. Hurrell, and T. Xu, 2001: Tropical origins for recent North Atlantic climate change. *Science,* **292,** 90–92.

Kudela, R. M., and F. P. Chavez, 1996: Bio-optical properties in relation to an algal bloom caused by iron enrichment in the equatorial Pacific. *Geophys. Res. Lett.,* **23,** 3751–3754.

Lehodey, P., M. Bertignac, J. Hampton, A. Lewis, and J. Picaut, 1997: El Niño Southern Oscillation and tuna in the western Pacific. *Nature,* **389,** 715–718.

Lewis, M. R., M.-E. Carr, G. C. Feldman, W. Esias, and C. McClain, 1990: Influence of penetrating solar radiation on the heat budget of the equatorial Pacific Ocean. *Nature,* **347,** 543–545.

Linsley, B. K., L. Ren, R. B. Dunbar, and S. S. Howe, 2000a: El Niño Southern Oscillation (ENSO) and decadal-scale climate variability at 10°N in the eastern Pacific from 1893 to 1994: A coral-based reconstruction from Clipperton Atoll. *Paleoceanography,* **15,** 322–335.

——, G. M. Wellington, and D. P. Schrag, 2000b: Decadal sea surface temperature variability in the subtropical South Pacific from 1726 to 1997 A.D. *Science,* **290,** 1145–1148.

McPhaden, M. J., 1999: Genesis and evolution of the 1997-98 El Niño. *Science,* **283,** 950–954.

——, and B. A. Taft, 1988: Dynamics of seasonal and intraseasonal variability in the eastern equatorial Pacific. *J. Phys. Oceanogr.*, **18,** 55–67.

——, and Coauthors, 1998: The tropical ocean global atmosphere observing system: A decade of progress. *J. Geophys. Res.*, **103,** 14 169–14 240.

Morel, A., and D. Antoine, 1994: Heating rate within the upper ocean in relation to its bio-optical state. *J. Phys. Oceanogr.*, **24,** 1652–1665.

——, and S. Maritorena, 2001: Bio-optical properties of oceanic waters: A reappraisal. *J. Geophys. Res.*, **106,** 7163–7180.

Murtugudde, R., J. Beauchamp, and A. J. Busalacchi, 2002: Effects of penetrative radiation on the upper tropical ocean circulation. *J. Climate,* **15,** 470–486.

Nakamoto, S., S. Prasanna Kumar, J. M. Oberhuber, J. Ishizaka, K. Muneyama, and R. Frouin, 2001: Response of the equatorial Pacific to chlorophyll pigment in a mixed layer isopycnal ocean general circulation model. *Geophys. Res. Lett.,* **28,** 2021–2024.

Ohlmann, J. C., D. A. Siegel, and L. Washburn, 1998: Radiant heating of the western equatorial Pacific during TOGA-COARE. *J. Geophys. Res.*, **103,** 5379–5395.

——, ——, and C. D. Mobley, 2000: Ocean radiant heating. Part I: Optical influences. *J. Phys. Oceanogr.*, **30,** 1833–1848.

Payne, R. E., 1972: Albedo of the sea surface. *J. Atmos. Sci.,* **29,** 959–970.

Paytan, A., M. Kastner, and F. P. Chavez, 1996: Glacial to interglacial fluctuations in productivity in the equatorial Pacific as indicated by marine Barite. *Science,* **274,** 1355–1357.

Picaut, J., F. Masia, and Y. du Penhoat, 1997: An advective-reflective conceptual model for the oscillatory nature of ENSO. *Science,* **277,** 663–666.

Rochford, P. A., A. B. Kara, A. J. Wallcraft, and R. A. Arnone, 2001: Importance of solar subsurface heating in ocean general circulation models. *J. Geophys. Res.*, **106,** 30 923–30 938.

Ryan, J. P., P. S. Polito, P. G. Strutton, and F. P. Chavez, 2002: Unusual large-scale phytoplankton blooms in the equatorial Pacific. *Progress in Oceanography,* Vol. 55, Pergamon, 263–285.

Sathyendranath, S., A. D. Gouveia, S. R. Shetye, P. Ravindran, and T. Platt, 1991: Biological control of surface temperature in the Arabian Sea. *Nature,* **349,** 54–56.

Siegel, D. A., J. C. Ohlmann, L. Washburn, R. R. Bidigare, C. T. Nosse, E. Fields, and Y. Zhou, 1995: Solar radiation, phytoplankton pigments and the radiant heating of the equatorial Pacific warm pool. *J. Geophys. Res.*, **100,** 4885–4891.

——, T. K. Westberry, and J. C. Ohlmann, 1999: Cloud color and ocean radiant heating. *J. Climate,* **12,** 1101–1116.

Smith, R. C. and K. S. Baker, 1978: The bio-optical state of ocean waters and remote sensing. *Limnol. Oceanogr.*, **23,** 247–259.

Strutton, P. G. and F. P. Chavez, 2000: Primary productivity in the equatorial Pacific during the 1997–98 El Niño. *J. Geophys. Res.*, **105,** 26 089–26 101.

Timmermann, A., and E.-F. Jin, 2003: Phytoplankton influences on tropical climate. *Geophys. Res. Lett.*, **29,** 2104, doi:10.1029/2002GL015434.

Wang, T., 1993: Satellite-derived long term net solar radiation over the global ocean surface: Its relationship to low frequency SST variation and El Niño. M.A. thesis, Department of Geography, University of California, Santa Barbara, 97 pp.

Wang, W., and M. J. McPhaden, 1999: The surface layer heat balance in the equatorial Pacific Ocean. Part I: Mean seasonal cycle. *J. Phys. Oceanogr.,* **29,** 1812–1831.

——, and ——, 2000: The surface layer heat balance in the equatorial Pacific Ocean. Part II: Interannual variability. *J. Phys. Oceanogr.,* **30,** 2898–3008.

——, and ——, 2001a: Surface layer temperature balance in the equatorial Pacific during the 1997/98 El Niño and 1998/99 La Niña. *J. Climate,* **14,** 3393–3407.

——, and ——, 2001b: What is the mean seasonal cycle of surface heat flux in the equatorial Pacific? *J. Geophys. Res.,* **106,** 837–857.

Wells, M. L., G. K. Vallis, and E. A. Silver, 1999: Tectonic processes in Papua New Guinea and past productivity in the eastern equatorial Pacific Ocean. *Nature,* **398,** 601–604.

White, W. B., D. R. Cayan, M. D. Dettinger, and G. Auad, 2001: Sources of global warming in upper ocean temperature during El Niño. *J. Geophys. Res.*, **106,** 4349–4367.

Wolter, K., and M. S. Timlin, 1998: Measuring the strength of ENSO—How does 1997/98 rank? *Weather,* **53,** 315–324.

Zhang, R.-H., L. M. Rothstein, and A. J. Busalacchi, 1998: Origin of the upper-ocean warming and El Niño change on decadal scales in the tropical Pacific Ocean. *Nature,* **391,** 879–883.